Macromolecular Research

Article

DOI 10.1007/s13233-021-9103-7

www.springer.com/13233 pISSN 1598-5032 eISSN 2092-7673

Thickness Effect of Polar Polymer Films on the Characteristics of Organic Memory Transistors

Chulyeon Lee[1]
Woongki Lee[1]
Hwajeong Kim[1,2]
Youngkyoo Kim*[,1]

[1] Organic Nanoelectronics Laboratory and KNU Institute for Nanophotonics Applications (KINPA), Department of Chemical Engineering, School of Applied Chemical Engineering, Kyungpook National University, Daegu 41566, Korea
[2] Priority Research Center, Research Institute of Environmental Science & Technology, Kyungpook National University, Daegu 41566, Korea

Received September 28, 2021 / Revised November 29, 2021 / Accepted November 30, 2021

Abstract: Organic memory transistors based on an organic field-effect transistor (OFET) structure were fabricated by employing a water-soluble polar polymer, poly(2-acrylamido-2-methyl-1-propanesulfonic acid) (PAMPSA). The thickness of PAMPSA films was varied from 180 nm to 1000 nm and thermally annealed (treated) at 170 ℃ for 30 min. The annealed PAMPSA films were optically transparent with naked eyes even though the absorbance at the wavelength range of *ca.* 190~260 nm gradually increased with the film thickness. The devices with the annealed PAMPSA films showed p-channel transistor characteristics at low operation voltages (0~-5 V) and delivered hysteresis of drain current due to the carbon radical-induced dipoles in the thermally annealed PAMPSA films. The best hysteresis characteristics were obtained at the film thickness of 450 nm, whereas the drain current was gradually decreased with the thickness of PAMPSA films. This result has been assigned to the trade-off effect between the capacitance decrease and the dipole increase the PAMPSA thickness increases. The optimized memory devices with the 450 nm-thick PAMPSA layers disclosed excellent retention characteristics during >10,000 cycles of writing-reading-erasing-reading memory tests.

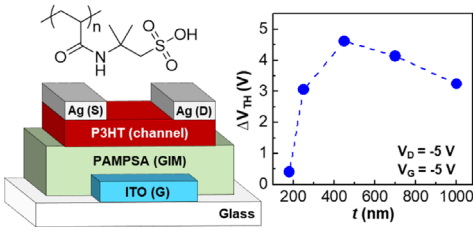

Keywords: organic memory transistor, OFET, polar polymer, thickness effect, hysteresis.

1. Introduction

Memory devices, which store information in a form of digital data, have been gradually developed on the basis of inorganic semiconductor technology.[1-3] Very recent advances in inorganic memory devices uncovered that three-dimensional stacking of transistors (>170 stages) on *ca.* 3~10 nm scale could greatly enhance the memory capacity per area, leading to much smaller memory modules including solid state devices (SSDs).[4-6] Taking it into account the memory capacity per volume only, quantum memory devices dealing with qubits are expected to take a major position in the future.[7-9] However, these memory devices have a limitation in terms of shape freedom such as bendability, flexibility and rollability because their core constituents consist of inorganic materials with rigid and hard characteristics.[10-12]

On this account, organic memory devices have been highlighted because organic materials can be bendable and flexible thanks to weak intermolecular forces among molecules.[13-15] In addition, polymers provide high toughness due to their long chains connected by covalent bonds and can be processed into thin films *via* wet-coating methods at room temperature, even though conventional inorganic memory devices require high temperature and vacuum processes.[16-20] These advantages of polymers have motivated polymer-based organic memory devices, specifically using organic field-effect transistor (OFET) geometry owing to the benefit of three electrodes in transistors, leading to transistor-type organic memory devices (TOMDs) in a broad context.[21-25]

For the fabrication of polymer-based TOMDs, conjugated polymers with a reasonable charge carrier mobility, such as poly(3-hexylthiophene) (P3HT), have been used as a channel layer in the geometry of OFET devices.[26-29] To achieve memory phenomenon, however, hysteresis characteristics of device current are essential at low voltages for practical applications. To date, very limited polymers, such as poly(vinyl alcohol) (PVA) and poly(2-acrylamido-2-methyl-1-propanesulfonic acid) (PAMPSA), were able to deliver both good hysteresis and low-voltage operation in the polymer-based TOMDs.[30-34] In the case of PAMPSA, it has been reported that thermal decomposition of PAMPSA side chain units can form carbon radical-induced dipoles leading to large-scale hysteresis in transistor characteristics.[35] However, no study has been reported on the influence of PAMPSA thickness even though the thickness of memory layers can affect the hysteresis characteristics of transistors.[36-38]

In this work, we have studied the thickness effect of PAMPSA films on the performance of polymer-based TOMDs. To fabri-

Acknowledgment: This work was financially supported by the National Research Foundation (NRF) of Korea (2021R1I1A3A04037494, 2021-R1I1A1A01060041, Basic Science Research Program_2018R1A6A1A-03024962) and the Ministry of Trade, Industry and Energy (MOTIE)-Korea Institute for Advancement of Technology (KIAT) through the International Cooperative R&D program (Project No. P0011262).

***Corresponding Author:** Youngkyoo Kim (ykimm@knu.ac.kr)

cate OFET devices, the PAMPSA films with various thicknesses (180 nm~1000 nm) were spin-coated on gate electrode-coated substrates and thermally annealed at 170 ℃ for 30 min before placing P3HT channel layers. Results showed that the hysteresis characteristics of devices were noticeably changed with the thickness of PAMPSA layers. The best hysteresis was achieved for the OFETs with the PAMPSA layers at the PAMPSA thickness (t) of 450 nm, whereas the highest current was measured at t = 180 nm. The optimized TOMDs with the 450 nm-thick PAMPSA layers exhibited stable memory characteristics with excellent retentions during >10,000 cycles at low voltages (0~-5 V).

2. Experimental

2.1. Materials and solutions

The PAMPSA polymer, which has a weight-average molecular weight of 2,000 kDa, was purchased from Sigma-Aldrich (St Louis, Mo, USA). To control the film thickness, the solid concentration of PAMPSA solutions was adjusted to 100, 200, 500, 700 and 1000 mg/mL by using deionized water as a solvent. All PAMPSA solutions were subjected to continuous stirring at room temperature for 3 days prior to spin-coating processes. The P3HT polymer, which has a weight-average molecular weight of 70 kDa, polydispersity index (PDI) of 1.7 and a regioregularity of 97%, was supplied from Rieke Metals (Lincoln, NE, USA). The P3HT solutions were prepared using toluene at a solid concentration of 12.5 mg/mL.

2.2. Film and device fabrication

Indium-tin oxide (ITO)-coated glasses (sheet resistance = *ca.* 10 Ω/cm^2) were used as a gate electrode-coated substrate for the present devices. A photolithography-etching process was employed to make the ITO electrodes patterned into small-sized ITO stripes (1 mm × 12 mm) that were used as a bottom gate electrode. The patterned ITO-glass substrates were washed first by immersing into acetone and cleaned in an ultrasonic bath for 30 min, followed by the same wet-cleaning process in isopropyl alcohol for 30 min. A gentle nitrogen flow was applied to dry the wet-cleaned ITO-glasses and then the dried ITO surfaces were subjected to UV-ozone treatment for *ca.* 20 min (UV intensity = 28 mW/cm^2). On top of the UV-ozone-treated ITO-glass substrates, the PAMPSA solutions were spun to make corresponding thin films. The thickness of PAMPSA films was 180, 250, 450, 700 and 1000 nm. The PAMPSA-coated ITO-glass substrates were thermally annealed at 170 ℃ for 30 min. Next, the P3HT solutions were spun on the thermally annealed PAMPSA layers (at 1500 rpm for 30 s) and soft-baked at 70 ℃ for 15 min. The thickness of P3HT layers was 60 nm. The P3HT-coated samples were mounted on a shadow mask and transferred into a vacuum chamber system equipped inside a nitrogen-filled glove box, followed by deposition of 60 nm-thick silver (Ag) source/drain electrodes at a base pressure of *ca.* 1 × 10^{-6} torr. The devices with the Ag electrodes featured a channel length (L) of 70 μm and a channel width (W) of 2 mm. All films and devices were wrapped and safely stored inside an argon-filled glovebox in order to avoid any attack from moisture and oxygen. For the measurement of ESR spectroscopy, the PAMPSA films (width: 3 mm, length: 20 mm) were coated on a polyimide film substrate and thermally annealed at 170 ℃ for 30 min. The metal-insulator-metal (MIM)-structured devices (glass/ITO/PAMPSA/Ag) with a parallel plate geometry were fabricated for the capacitance measurement of PAMPSA films.

2.3. Measurements

The thickness of polymer films and metal electrodes was measured using a surface profilometer (DektakXT, Bruker, USA), while the optical absorption spectra of polymer films were measured using a UV/VIS/NIR spectrometer (Lambda 750, Perkin-Elmer, Houston, TX, USA). The frequency-dependent capacitances of MIM devices (glass/ITO/PAMPSA/Ag) were measured using an impedance spectrometer (Versa STAT 4, Ametek Scientific Instruments) at a bias voltage of 0 V (rms). The existence of radicals in the PAMPSA films was investigated using an electron spin resonance (ESR) spectrometer (EMXplus-9.5/2.7, Bruker, USA). The surface morphology of polymer film samples was measured using an atomic force microscope (AFM, Scanning Probe Microscope NX20, Park Systems, South Korea). The performance and memory characteristics of OFETs were measured using a semiconductor parameter analyzer (4200 SCS and 2636 B, Keithley, USA). A home-built sample holder, which is filled with argon gas, was used for the measurement of devices in an inert condition.

3. Results and discussion

The PAMPSA layers with various thicknesses (t = 180~1000 nm), which were thermally annealed at 170 ℃ for 30 min, were placed as a gate insulating memory (GIM) layer between the P3HT channel layers and the ITO gate electrodes in the OFETs with a transistor geometry of bottom gate and top source/drain electrodes (see Figure 1(a)). As shown in Figure 1(b), all the annealed PAMPSA films delivered two distinguished absorption peaks below a wavelength (λ) of *ca.* 260 nm. The main absorption peak was slightly redshifted from λ = 200 nm to λ = 215 nm

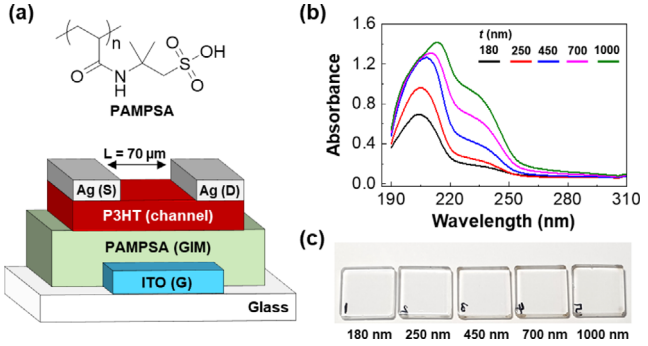

Figure 1. (a) Device structure for the OFET with the PAMPSA layer (see the chemical structure of PAMPSA on the top). (b) Optical absorption spectra of the PAMPSA films coated on quartz substrates (thermal treatment at 170 ℃ for 30 min) according to the PAMPSA thickness (t). (c) Photograph for the PAMPSA films coated on quartz substrates (thermal treatment at 170 ℃ for 30 min).

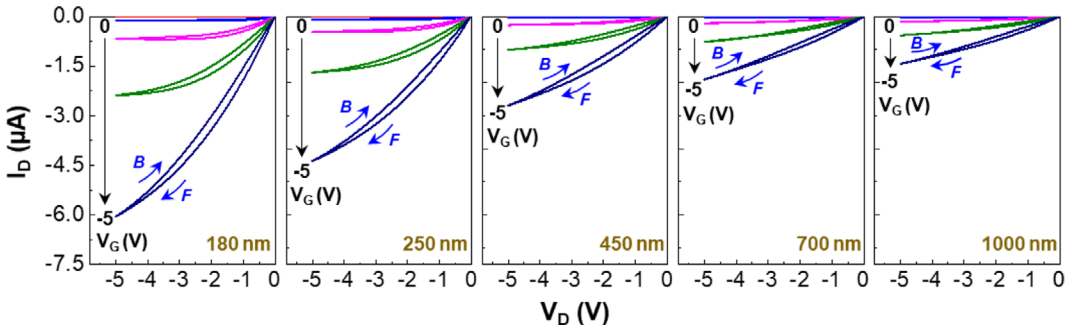

Figure 2. Output characteristics (dark condition) for the OFETs with the PAMPSA layers according to the PAMPSA thickness (t). '*F*' and '*B*' denote forward and backward sweeps, respectively.

as the PAMPSA thickness increased, whereas the shoulder peak was almost unchanged with the PAMPSA thickness. The spectral shift for the main absorption peak can be attributed to the influence of thermal annealing that evolves dissociation of side groups in the PAMPSA chains (see the spectral shift by thermal annealing in Figure S1).[25] In detail, the thermally dissociated parts in films might be gradually increased as the PAMPSA thickness increased, leading to the gradual redshift of absorption peaks with the PAMPSA thickness. As a consequence, the annealed PAMPSA films exhibited high optical transparency in the visible range (see Figure 1(c)).

As shown in the output curves (see Figure 2), all devices exhibited typical p-channel transistor characteristics at a low drain voltage (V_D) range of 0~-5 V and delivered gradually increased drain current (I_D) by increasing the gate voltage (V_G) up to -5 V. Interestingly, the drain current at the same drain and gate voltages was gradually decreased as the PAMPSA thickness increased (see Figure S2). This result can be basically ascribed to the higher capacitances at the thinner films when it comes to the relationship, $C = (\varepsilon \times A)/t$, where C, ε, and A stand for capacitance, dielectric constant, and area, respectively, if the same voltage is applied.[39,40] Here it is noted that very small hysteresis in drain current was measured from the output curves regardless of the PAMPSA thickness. This may reflect that no charge trapping sites were evolved in the P3HT channel layers and/or the interfaces between the P3HT channel layers and the PAMPSA layers.

To further understand the transistor characteristics, the transfer curves of devices were measured and compared according to the PAMPSA thickness. As shown in Figure 3, all devices delivered typical transfer curves of p-channel transistors. The drain current at V_G = -5 V was gradually reduced as the PAMPSA thickness increased (see Figure S3), which in good agreement with the trend of output curves, whereas the off-current level was gradually increased with the PAMPSA thickness. This result can be explained by the increased gate leakages, as supported by the gradual increase in gate current (I_G) with the PAMPSA thickness, which is partly ascribed to the relatively higher (poorer) surface roughness for the thicker PAMPSA layers (see Figure S4). In addition, the gradual decrease in drain current might be also made by the reduced polarization effect owing to the relatively lower electric field for the thicker PAMPSA layers. However, the gate voltage sweep test uncovered that all devices exhibited a noticeable hysteresis behavior that is dependent on the PAMPSA thickness. Apparently, it is observed that the hysteresis (i.e., voltage difference at the same level of drain current) seemed to be larger as the PAMPSA thickness increased up to t = 450 nm and then became slightly smaller by further increase of PAMPSA thickness.

The detailed trend of hysteresis, which is represented by the threshold voltage shift (ΔV_{TH}) between forward and backward transfer curves, is plotted as a function of PAMPSA thickness in Figure 4(a). Here the best ΔV_{TH} value was obtained at the PAMPSA thickness of t = 450 nm. Here it is noted that the on/off ratio of devices became gradually poor with the PAMPSA thickness. In addition, as seen from Figure 4(b), the hole mobility (forward sweep) was relatively decreased as the PAMPSA thickness increased. This result can be attributed to the reduced drain current caused by the thickness-induced lowering of charge carrier generation in the P3HT channel layers, as evidenced by the similar trend of capacitances with the PAMPSA thickness (see Figure S5). The related parameters are summarized in

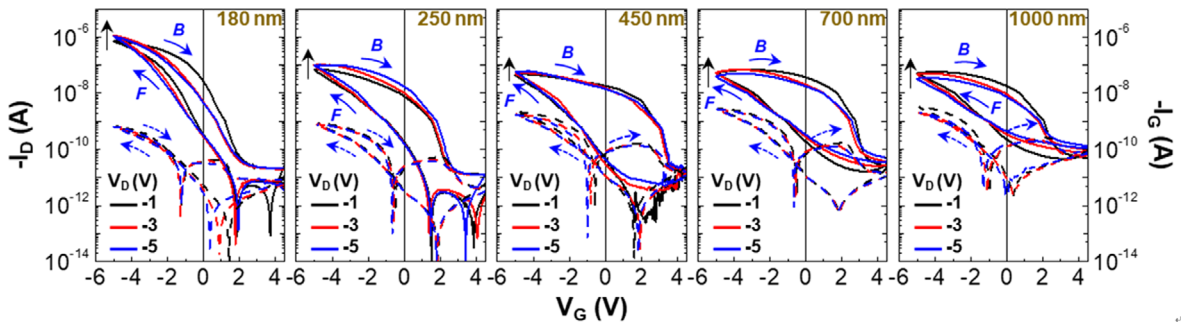

Figure 3. Transfer characteristics (dark condition) for the OFETs with the PAMPSA layers according to the PAMPSA thickness (t): (solid lines) I_D-V_G curves, (dashed lines) I_G-V_G curves. '*F*' and '*B*' denote forward and backward sweeps, respectively.

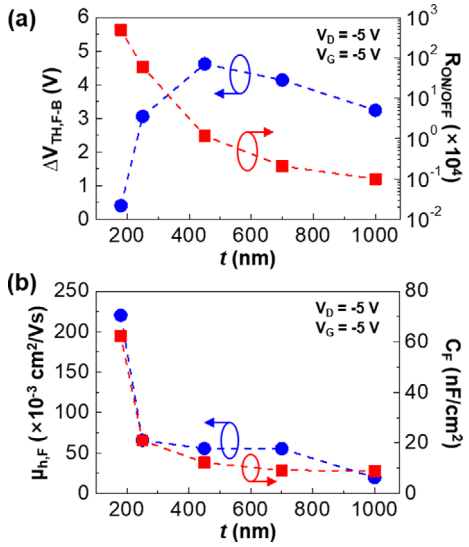

Figure 4. (a) Threshold voltage shift ($\Delta V_{TH,F-B}$) and on/off ratio ($R_{ON/OFF}$) as a function of PAMPSA thickness. (b) Hole mobility ($\mu_{h,F}$) and capacitance (C_F) as a function of PAMPSA thickness. All data were extracted from the transfer curves in Figure 2.

Table 1.

As observed in our previous report, the present hysteresis phenomenon can be assigned to the formation of carbon radical-induced dipoles in the PAMPSA chains by thermal decomposition process.[27] However, it is the first time to disclose the strong dependence of PAMPSA thickness on the hysteresis phenomenon. In principle, the amount of carbon radical-induced dipoles should be higher as the PAMPSA thickness increased. This simple consideration gives that the thicker the PAMPSA thickness, the larger the hysteresis of devices. This is evidenced from the ESR signals at around 3350 G which became higher at the thicker PAMPSA layers (see Figure 5). However, as we mentioned above, the relationship between thickness and capacitance strongly affected the population of charge carriers formed in the P3HT channel layers so that the best hysteresis was achieved at t = 450 nm *via* trade-off effect between capacitance and radical formation.

Finally, the performance as a memory device was tested by applying a writing-once-reading-many (WORM) algorithm. As shown in Figure 6(a), a stable reading signal (drain current at V_G = -1.5 V and V_D = -5 V) was measured after writing once (V_G = -5

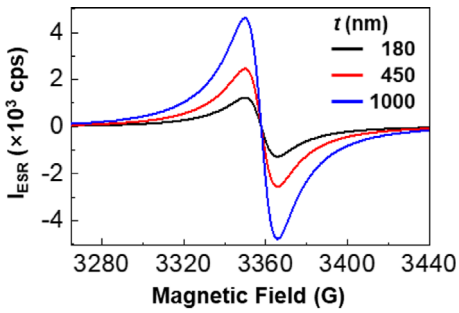

Figure 5. ESR spectra for the PAMPSA films according to the PAMPSA film thickness (t). The details of ESR measurement are given in the experimental section.

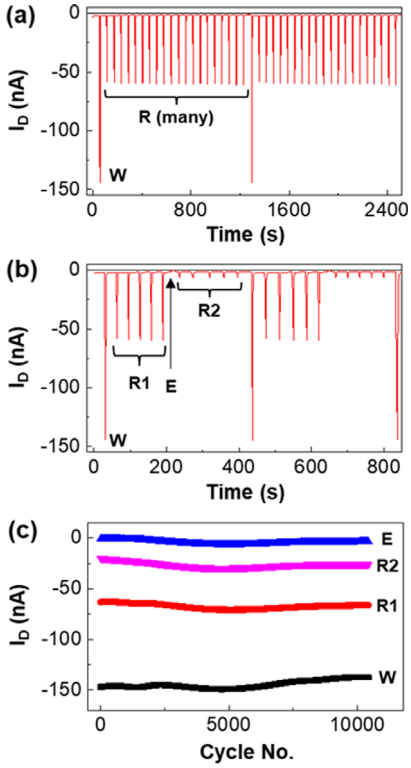

Figure 6. (a) Writing-once-reading-many (WORM) operation results for the OFETs with the PAMPSA layers (t = 450 nm) [W: V_G = -5 V and V_D = -5 V; R: V_G = -1.5 V and V_D = -5 V]. (b) Writing-reading-erasing-reading (WRER) operation results for the OFETs with the PAMPSA layers (t = 450 nm) [W: V_G = -5 V and V_D = -5 V; R1, R2: V_G = -1.5 V and V_D = -5 V; E: V_G = +5 V and V_D = -5 V]. (c) Retention characteristics during 10,420 WRER cycles at the same operation condition as used for (b).

Table 1. Summary of transistor characteristics for the OFETs with the PAMPSA layers according to the PAMPSA thickness (t). Note that all parameters were extracted from transfer curves.

Parameters	t (nm)				
	180	250	450	700	1000
$I_{D,Max,F}$[a] (μA)	-6.06	-4.37	-2.69	-1.91	-1.43
$\mu_{h,F}$[b] (×10⁻³ cm²/Vs)	2.23	0.66	0.56	0.55	0.19
C_F[c] (nF/cm²)	62.37	20.88	12.21	9.19	8.87
$R_{ON/OFF}$[d] (×10⁴)	489.82	60.06	1.19	0.21	0.10
$V_{TH,F}$[e] (V)	-1.09	-1.12	-1.13	-1.16	-0.92
$V_{TH,B}$[f] (V)	-0.68	1.94	3.49	3.01	2.32
$\Delta V_{TH,F-B}$[g] (V)	0.41	3.06	4.62	4.17	3.24

[a]Maximum drain current at V_G = V_D = -5 V (forward sweep). [b]Hole mobility (forward sweep). [c]Capacitance of PAMPSA film. [d]On/off ratio (forward sweep). [e]Threshold voltage (forward sweep). [f]Threshold voltage (backward sweep). [g]Threshold voltage shift (between forward and backward sweeps).

V and V_D = -5 V) for the OFETs with the 450 nm-thick PAMPSA layers. Next, a writing-reading-erasing-reading (WRER) operation was performed for the optimized OFETs with the 450 nm-thick PAMPSA layers. After writing (W) at V_G = -5 V and V_D = -5 V, the reading signal (R1) was clearly measured at V_G = -1.5 V and V_D = -5 V. After the erasing (E) operation was applied at V_G = +5 V and V_D = -5 V, the subsequent reading (R2) at V_G = -1.5 V and V_D = -5 V delivered relatively lower drain current than R1 (see Figure 6(b)). This operation confirms that the present OFETs do certainly function as a memory device. By applying the same WRER algorithm, the present OFETs exhibited excellent retention characteristics over 10,420 cycles (see Figure 6(c)). Considering these stable memory functions at low voltages, the present TOMDs with the 450 nm-thick PAMPSA layers have strong advantages over other types of organic memory transistors with floating gates *etc*.[41,42]

4. Conclusions

The PAMPSA thin films with various thicknesses were applied as a gate-insulating memory layer for polymer-based transistor-type organic memory transistors. All the thermally annealed PAMPSA films exhibited two characteristic peaks of optical absorption in the range of UV light (< λ = 260 nm) without respect to the film thickness, but the main absorption peak (< λ = 200 nm) was gradually redshifted with the film thickness. The OFETs with the PAMPSA layers could be operated with typical p-channel mode at low voltages (0∼-5 V) regardless of the PAMPSA thickness. However, as the PAMPSA thickness increased, the drain current of devices was gradually decreased because of the capacitance – thickness relationship. The transfer curves resulted in hysteresis characteristics for all devices, but the best hysteresis was achieved at the PAMPSA thickness of t = 450 nm due to the trade-off between decreasing capacitances and increasing dipoles by increasing the PAMPSA thickness. The optimized OFETs with the PAMPSA layers (t = 450 nm) showed outstanding memory retention characteristics up to 10,420 WRER cycles at low voltages (programming range = -5 V∼+5 V).

Supporting information: Information about comparison of spectral shift in optical absorption spectra, drain current change according to the film thickness from output and transfer curves, and frequency-dependent capacitance changes. The materials are available *via* the Internet at http://www.springer.com/13233.

References

(1) W.-C. Chen, *Electrical memory materials and devices*, RSC Publishing, 2015.
(2) X. Shi, H. Chen, F. Hao, R. Liu, T. Wang, P. Qiu, U. Burkhardt, Y. Grin, and L. Chen, *Nat. Mater.*, **17**, 421 (2018).
(3) O. Tizno, A. Marshall, N. Fernández-Delgado, M. Herrera, S. Molina, and M. Hayne, *Sci. Rep.*, **9**, 8950 (2019).
(4) X. Yao, K. Klyukin, W. Lu, M. Onen, S. Ryu, D. Kim, N. Emond, I. Waluyo, A. Hunt, J. Alamo, J. Li, and B. Yildiz, *Nat. Commun.*, **11**, 3134 (2020).
(5) J. Liang, C. Jiang, and W. Wu, *Nanoscale*, **11**, 7041 (2019).
(6) B. Pandit, B. Sankapal, and P. Koinkar, *Sci. Rep.*, **9**, 5892 (2019).
(7) K. T. Kaczmarek, P. M. Ledingham, B. Brecht, S. E. Thomas, G. S. Thekkadath, O. Lazo-Arjona, J. H. D. Munns, E. Poem, A. Feizpour, D. J. Saunders, J. Nunn, and I. A. Walmsley, *Phys. Rev. A*, **97**, 042316 (2018).
(8) T. Zhong, J. Kindem, J. Bartholomew, J. Rochman, I. Craiciu, E. Miyazono, M. Bettinelli, E. Cavalli, V. Verma, S. Nam, F. Marsili, M. Shaw, A. Beyer, and A. Faraon, *Science*, **357**, 1392 (2017).
(9) P. Vernaz-Gris, K. Huang, M. Cao, A. Sheremet, and J. Laurat, *Nat. Commun.*, **9**, 363 (2018).
(10) S. Huang, Y. Liu, M. Jafari, M. Siaj, H. Wang, S. Xiao, and D. Ma, *Adv. Funct. Mater.*, **31**, 2010022 (2021).
(11) S. Lai, I. Temino, T. Cramer, F. Pozo, B. Fraboni, P. Cosseddu, A. Bonfiglio, and M. Mas-Torrent, *Adv. Electron. Mater.*, **4**, 1700271 (2018).
(12) B. Che, D. Zhou, H. Li, C. He, E. Liu, and X. Lu, *Org. Electron.*, **66**, 86 (2019).
(13) Z. Jin, Y. Chen, Q. Zhou, P. Mao, H. Liu, J. Wang, and Y. Li, *Mater. Chem. Front.*, **1**, 1338 (2017).
(14) P. Zhang, B. Xu, C. Gao, G. Chen, and M. Gao, *ACS Appl. Mater. Interfaces*, **8**, 30336 (2016).
(15) S. Bhattacharjee, U. Das, P. Sarkar, and A. Roy, *Org. Electron.*, **58**, 145 (2018).
(16) C. Lee, H. Kim, and Y. Kim, *npj Flex. Electron.*, **5**, 10 (2021).
(17) C. Lee, H. Kim, and Y. Kim, *ACS Appl. Mater. Interfaces*, **13**, 16 (2021).
(18) S. Mondal, and V. Venkataraman, *Nat. Commun.*, **10**, 2143 (2019).
(19) Y. Yang, G. Yuan, Z. Yan, Y. Wang, X. Lu, and J. Liu, *Adv. Mater.*, **29**, 1700425 (2017).
(20) S. Mondal, and V. Venkataraman, *Appl. Phys. Lett.*, **114**, 173502 (2019).
(21) C. Lo, Y. Watanabe, D. Murakami, C. Shih, K. Nakabayashi, H. Mori, and W. Chen, *Macromol. Rapid Commun.*, **40**, 1900115 (2019).
(22) C. Zheng, T. Tong, Y. Hu, Y. Gu, H. Wu, D. Wu, H. Meng, M. Yi, J. Ma, D. Gao, and W. Huang, *Small*, **14**, 1800756 (2018).
(23) S. Nam, Y.-G Ko, S. Hahm, S. Park, J. Seo, H. Lee, H. Kim, M. Ree, and Y. Kim, *NPG Asia Mater.*, **5**, e33 (2013).
(24) S. Lee, K. Cho, S. Jung, S. Kim, J. Lee, and K. Lee, *Macromol. Res.*, **28**, 683 (2020).
(25) O. Gunaydin, A. Demir, G. Demir, I. Yucedag, and B. Cosut, *Macromol. Res.*, **26**, 164 (2018).
(26) C. Lee, J. Jeong, H. Kim, and Y. Kim, *J. Hazard. Mater.*, **374**, 159 (2019).
(27) B. Nketia-Yawson, and Y.-Y. Noh, *Macromol. Res.*, **25**, 489 (2017).
(28) H. Han, C. Lee, H. Kim, and Y. Kim, *Adv. Funct. Mater.*, **28**, 1800704 (2018).
(29) G. V. Leite, E. A. Van Etten, M. M.C. Forte, and H. Boudinov, *Synth. Met.*, **229**, 33 (2017).
(30) J. Seo, S. Nam, H. Kim, T. D. Anthopoulos, D. D. C. Bradley, and, Y. Kim, *NPG Asia Mater.*, **8**, e235 (2016).
(31) Y. Sun, J. Lu, C. Ai, and D. Wen, *Phys. Chem. Chem. Phys.*, **18**, 11341 (2016).
(32) C. Lee, J. Jeong, H. Kim, and Y. Kim, *Mater. Horiz.*, **6**, 1899 (2019).
(33) J. J. L. Hmar, *RSC Adv.*, **8**, 20423 (2018).
(34) J. Seo, H. Kim, C. Lee, and Y. Kim, *Adv. Electron. Mater.*, **6**, 1900920 (2020).
(35) C. Lee, J. Jeong, H. Kim, and Y. Kim, *ACS Appl. Mater. Interfaces*, **11**, 48113 (2019).
(36) S. Chandrasekaran, F. Simanjuntak, R. Aluguri, and T.-Y. Tseng, *Thin Solid Films*, **660**, 777 (2018).
(37) T. Park, S. Song, H. Kim, S. Kim, S. Chung, B. Kim, K. Lee, K. Kim, B. Choi, and C. Hwang, *Sci. Rep.*, **5**, 15965 (2015).
(38) H. Ling, W. Li, H. Li, M. Yi, L. Xie, L. Wang, Y. Ma, Y. Bao, F. Guo, and W. Huang, *Org. Electron.*, **43**, 222 (2017).
(39) H. Park, J. Roh, Y. Lee, and C. Hwang, *Adv. Mater.*, **31**, 1805266 (2019).
(40) C. Van Dyck, T. J. Marks, and M. A. Ratner, *ACS Nano*, **11**, 5970 (2017).
(41) Y. Chiang, C. Hung, Y. Lin, Y. Chiu, T. Isono, T. Satoh, W. Chen, *Adv. Mater.*, **32**, 2002638 (2020).
(42) Q. Li, T. Li, Y. Zhang, Z. Chen, Y. Li, L. Jin, H. Zhao, J. Li, J. Yao, *J. Phys. Chem. C*, **124**, 23343 (2020).